In vitro anticancer effect of azithromycin targeting hypoxic lung cancer cells via the inhibition of mitophagy

KAZUTOSHI TORIYAMA[1,2], TAKASHI OKUMA[1,2], SHINJI ABE[2], HIROYUKI NAKAMURA[1] and KAZUTETSU AOSHIBA[1]

[1]Department of Respiratory Medicine, Tokyo Medical University Ibaraki Medical Center, Ami-machi, Ibaraki 300-0395; [2]Department of Respiratory Medicine, Tokyo Medical University, Tokyo 160-0023, Japan

Received May 11, 2023; Accepted October 18, 2023

DOI: 10.3892/ol.2023.14146

Abstract. Solid tumors are predisposed to hypoxia, which induces tumor progression, and causes resistance to treatment. Hypoxic tumor cells exploit auto- and mitophagy to facilitate metabolism and mitochondrial renewal. Azithromycin (AZM), a widely used macrolide, inhibits autophagy in cancer cells. The aim of the present study was to determine whether AZM targeted hypoxic cancer cells by inhibiting mitophagy. Lung cancer cell lines (A549, H1299 and NCI-H441) were cultured for up to 72 h under normoxic (20% O_2) or hypoxic (0.3% O_2) conditions in the presence or absence of AZM (≤25 μM), and the cell survival, autophagy flux and mitophagy flux were evaluated. AZM treatment reduced cell survival under hypoxic conditions, caused mitolysosome dysfunction with raised lysosomal pH and impaired the efficient removal of hypoxia-damaged mitochondria, eventually inducing apoptosis in the cancer cells. The cytotoxic effect of AZM under hypoxic conditions was abolished in mitochondria-deficient A549 cells (ρ^0 cells). The present study demonstrated that AZM reduced lung cancer cell survival under hypoxic conditions by interfering with the efficient removal of damaged mitochondria through mitophagy inhibition. Thus, AZM may be considered as a promising anticancer drug that targets the mitochondrial vulnerability of hypoxic lung cancer cells.

Correspondence to: Professor Kazutetsu Aoshiba, Department of Respiratory Medicine, Tokyo Medical University Ibaraki Medical Center, 3-20-1 Chuou, Inashiki-gun, Ami-machi, Ibaraki 300-0395, Japan
E-mail: kaoshiba@tokyo-med.ac.jp

Abbreviations: AZM, azithromycin; BNIP3, Bcl-2/E1B-19kDa interacting protein 3; BNIP3L/Nix, Bcl-2/E1B-19kDa interacting protein 3-like; Em, emission wavelength; Ex, excitation wavelength; HIF, hypoxia-inducible factor; HSP 60, heat shock protein 60; LMP, lysosomal membrane permeabilization; MMP, mitochondrial membrane potential; TME, tumor microenvironment; TMRM, tetramethylrhodaminemethyl ester; UQCRC1, ubiquinol-cytochrome β-c1 complex subunit 1

Key words: autophagy, mitophagy, AZM, hypoxia, TME

Introduction

Tumor cells are characterized by hypoxia, with pO_2 levels reaching up to <10 mmHg at the center of a solid tumor (1,2). The lack of vascularity leads to a mismatch between oxygen delivery and consumption and is thought to be the main cause of tumor hypoxia. Subsequently, abnormal angiogenesis, tumor invasion, and metastasis are activated; additionally the frequently observed resistance to immune-, chemo-, and radiotherapies can contribute to tumor progression (3,4). Hence, tumor hypoxia is generally considered a promising target for cancer therapy (5,6).

Mounting evidence suggests that autophagy plays a pivotal role in maintaining tumor cell survival under hypoxic conditions. Autophagy is an intracellular self-degradative mechanism that is facilitated in response to environmental stressors, such as nutrient deficiency and hypoxia (7). Mitophagy is a selective form of autophagy that removes defective or excessive mitochondria from the cell. Recent studies have shown that tumor cells exploit both auto- and mitophagy to cope with reduced oxygen and metabolic supplies, control the neogenesis and functions of mitochondria, and promote cell survival in hypoxic tumor microenvironments (TMEs) (8,9). In this context, inhibiting auto- or mitophagy might prove beneficial in inducing tumor cell death in hypoxic TMEs. However, predominant autophagy that exceeds its adaptive capacity within the cell can facilitate tumor cell death (10,11); hence, the stimulation of auto- or mitophagy under hypoxic TME may provide an alternative therapeutic scheme. Nonetheless, the effect of inhibiting or stimulating auto- or mitophagy while targeting hypoxic tumor cells during anticancer therapy remains unclear.

Recent studies, including ours, have demonstrated that azithromycin (AZM), a widely used antibiotic belonging to the macrolide group, exhibits antiproliferative, pro-apoptotic, anti-autophagy, and anti-angiogenic effects in cancer cells (12). Furthermore, it can potentiate the anticancer effects of chemotherapeutic drugs, such as DNA-damaging chemotherapeutic agents, tyrosine kinase inhibitors, and proteasome inhibitors, by inhibiting autophagy (13-18). One study, in particular, outlined the involvement of AZM in cytoskeletal protein dynamics, which subsequently inhibited autophagy (19). Additionally, AZM is reported to inhibit mitochondrial ribosome in cancer

cells, thereby interfering with the process of mitophagy (20). Thus, the role of AZM is directly linked to enhancing apoptosis and exhibiting caspase 3/7, as demonstrated in glioblastoma and leukemia (21,22). In the present study, we hypothesized that AZM might specifically target hypoxic cancer cells by suppressing auto- and mitophagy for cancer cell survival under hypoxic conditions. To test this hypothesis, we extended our previous research to evaluate the effect of AZM on lung cancer cell survival under hypoxic and normoxic conditions.

Materials and methods

Cell culture. Human non-small cell lung cancer cell lines (A549, H1299, and NCI-H441) were obtained from the American Type Culture Collection (Manassas, VA, USA). A549 cells were maintained on bovine type I collagen-coated plates in Dulbecco's Modified Eagle medium (DMEM; Gibco; Thermo Fisher Scientific, Inc., Waltham, MA, USA) supplemented with 10% fetal bovine serum (FBS) and 1% penicillin/streptomycin (growth medium) at 37˚C in a humidified incubator (CO_2 incubator 900EX, Wakenyaku Co., Ltd., Tokyo, Japan) saturated with a gas mixture containing 5% CO_2 and 20% O_2. The H1299 and NCI-H441 cells were maintained on bovine type I collagen-coated plates in Roswell Park Memorial Institute (RPMI; Gibco) supplemented with 10% FBS and 1% penicillin/streptomycin. The A549 and H1299 cell lines were authenticated via short tandem repeat profiling, which was performed using the Promega PowerPlex® 16 HS system (Promega Corporation, Madison, WI). At 24 h prior to each experiment, the cells were replated on a new plate and grown in the relevant medium. Just before the experiment, A549 and H1299 cells were saturated with RPMI and supplemented with 1% FBS (serum-reduced experimental medium), while the NCI-H441 cells with RPMI were supplemented with 5% FBS. Thereafter, the cells were stored in a humidified incubator containing 5% CO_2 with either 20% O_2 (normoxia) or 0.3% O_2 (hypoxia) in the presence (5, 10, or 25 μM or 25 μM unless otherwise indicated) or absence of AZM (Tokyo Chemical Industry, Tokyo, Japan). In some experiments, the cells were incubated in the presence of Z-VAD-FMK (25 μM, Adooq Bioscience, Irvine, CA, USA).

Cell survival assay. Cell survival was evaluated in a 96-well flat-bottom culture plate using the Hoechst 33342 DNA quantification assay. Briefly, the cells were lysed in 100 μl of distilled water, followed by a freeze-thaw cycle. The cell lysates were then solubilized in 100 μl of TNE buffer (10-mM Tris, 1-mM EDTA, and 2-M NaCl; pH 7.4) containing 10 μg/ml of Hoechst 33342 (Sigma-Aldrich Japan, Tokyo, Japan). The fluorescence intensities were read at an excitation wavelength (Ex) of 350 nm and emission wavelength (Em) of 460 nm using a microplate fluorometer (PerkinElmer ArvoX2; PerkinElmer Japan Co., Ltd., Tokyo, Japan).

Cell morphology. Cells in an 8-chamber cell culture slide were stained with a Diff-quick solution (Agilent, Santa Clara, CA, USA) and examined under a Nikon Optiphot-2 microscope (Nikon Solutions Co., Ltd., Tokyo, Japan). Apoptotic cells were identified based on nuclear pyknosis or chromatin condensation and the cell shrinkage.

Western blotting. The cell samples were lysed in a radioimmunoprecipitation assay buffer (50-mM Tris hydrochloride, 150-mM NaCl, 0.4-mM EDTA, 0.5% Nonidet P-40, and 0.1% SDS; pH 7.4) supplemented with a protease inhibitor (#P8340; Sigma-Aldrich Japan) and a phosphatase inhibitor (#sc-45065; Santa Cruz Biotechnology, Santa Cruz, CA, USA) cocktail. The samples were centrifuged at 13,000 g for 10 min, and the total protein concentration in the supernatants was assessed using the DC protein assay kit (#5000112, Bio-Rad Laboratories). After adding 5X sample buffer (500-mM Tris, 5% 2-mercaptoethanol, 10% glycerin, 2.5% SDS, and 0.0125% bromophenol blue; pH 6.8), the samples with equal amounts of proteins were fractionated by SDS-polyacrylamide gel electrophoresis and transferred to a polyvinylidene difluoride membrane (EMD Millipore Immobilon®-P; Millipore, Co., Billerica, MA, USA). The membranes were blocked with 4% bovine serum albumin (BSA; Biowest), probed with the primary antibodies described below, diluted in an immunoreaction enhancer solution (Can Get Signal® Solution 1; Toyobo Co., Ltd., Osaka, Japan), and reacted with horseradish peroxidase (HRP)-conjugated secondary antibodies, such as stabilized goat anti-rabbit immunoglobulin (Ig) G (1:1,000; #32460, Thermo Fisher Scientific) and stabilized goat anti-mouse IgG (1:1,000; #32430, Thermo Fisher Scientific). The immune complexes were visualized using an enhanced chemiluminescence reagent (#34579, SuperSignal West Pico Plus; Thermo Fisher Scientific). The signal intensities were quantified by densitometric scanning using ImageJ (version 1.49V; National Institutes of Health, Bethesda, MD, USA).

The primary antibodies used in this study were rabbit polyclonal anti-poly (ADP-ribose) polymerase 1 (1:1,000; sc-7150, Santa Cruz Biotechnology), rabbit polyclonal anti-caspase-3/p17/p19 (1:1,000; 19677-1-AP, Proteintech Group, Inc., Rosemont, IL, USA), rabbit polyclonal anti-ubiquinol-cytochrome b-c1 complex subunit 1 (UQCRC1; 1:1,000; 21705-1-AP, Proteintech), rabbit polyclonal anti-p62 (1:1,000; 18420-1-AP, Proteintech, Rosemont, IL, USA), mouse monoclonal anti-heat shock protein 60 (HSP 60; 1:1,000; SPA-807, Stressgen Biotechnologies, San Diego, CA, USA), rabbit polyclonal anti-microtubule-associated protein 1 light chain 3B (LC3B; 1:1,000; NB600-1384, Novus Biologicals, Inc., Littleton, CO, USA), rabbit monoclonal anti-Bcl-2/E1B-19kDa interacting protein 3 (BNIP3; 1:1,000; #44060, Cell Signaling Technology, Danvers, MA, USA), rabbit monoclonal anti-Bcl-2/E1B-19kDa interacting protein 3-like (BNIP3L/Nix; 1:1,000; #12396, Cell Signaling Technology), and mouse monoclonal anti-β-actin conjugated with horseradish peroxidase (1:6,000; #017-24573, Fujifilm Wako Chemicals, Osaka, Japan).

Immunofluorescence staining. Cells in an 8-chamber cell culture slide were fixed with 3% paraformaldehyde and permeabilized with 0.5% Triton® X-100 (Nacalai Tesque, Inc., Kyoto, Japan) in PBS for 10 min. After blocking the nonspecific binding sites with 3% BSA, the slides were incubated with rabbit polyclonal anti-cleaved caspase-3 (Asp175) (1:100; #9661, Cell Signaling Technology), followed by alpaca anti-rabbit IgG (VHH) conjugated with Alexa Fluor 488 (1:1,000; SA510322, Thermo Fisher Scientific). The cell nuclei were then counterstained with 4',6-diamidino-2-phenylindole (DAPI), and fluorescence images were obtained using a Nikon Optiphot-2 microscope.

Assessment of the lysosomal pH. The lysosomal pH was assessed using the Lysosomal Acidic pH Detection kit (#L266; Dojindo Laboratories, Kumamoto, Japan), according to the manufacturer's instructions. Briefly, cells in an 8-chamber cell culture slide were loaded with pHLys®Red for 30 min at 37˚C, and fluorescence images were acquired using a Nikon Optiphot-2 microscope. The fluorescence intensity of pHLys®Red, which accumulates in intact lysosomes, increases with the increase in acidity, and only weak fluorescence is detected when lysosomes are neutralized.

Assessment of the auto- and mitophagy flux in live cells. Cells in an 8-chamber cell culture slide were loaded with DAP®Red (#D677, Dojindo Laboratories), which detected both autophagosomes and autolysosomes, and DAL®Green (#D676, Dojindo Laboratories), which detected only autolysosomes, for 30 min at 37˚C as per the manufacturer's instructions. DAL®Green and DAP®Red are generally incorporated in the autophagosome. The DAL®Green fluorescence becomes stronger after the fusion of the lysosome with the autophagosome, due to the increase in the acidity, whereas the DAP®Red fluorescence remains unchanged.

For the mitophagy flux, cells in an 8-chamber cell culture slide were loaded with Mtphagy®Dye (#MT01, Dojindo Laboratories) and Lyso®Dye (Dojindo Laboratories), which accumulate in intact mitochondria and lysosomes, respectively. When mitophagy is induced, the mitophagosomes fuse to lysosomes to form mitolysosomes, and the Mtphagy®Dye emits a strong red fluorescence due to the increase in acidity. Fluorescence images were obtained using a Nikon Optiphot-2 microscope.

Measurement of the oxygen consumption rate. The oxygen consumption rate was measured using a Seahorse XFp analyzer (Agilent, Santa Clara, CA) and an XFp Cell Mito Stress Test Kit (#103010-100, Agilent), according to the manufacturer's instructions (23).

Assessment of the mitochondrial membrane potential. Cells in an 8-chamber cell culture slide were loaded with the mitochondrial membrane potential (MMP) indicator, tetramethylrhodaminemethyl ester (TMRM); 250 nM; #T688, Thermo Fisher Scientific) for 30 min at 37˚C, and fluorescence images were acquired using a Nikon Optiphot-2 microscope. The cells were plated in a 96-well flat-bottom culture plate and stained with TMRM (250 nM) and Hoechst 33342 (2 μg/ml) for 30 min at 37˚C to quantify the MMP. The medium was substituted with PBS, and the fluorescence intensities of TMRM (Ex 530 nm, Em 600 nm) and Hoechst33342 (Ex 355 nm, Em 460 nm) were recorded on a microplate fluorometer. The TMRM fluorescence was normalized to that of Hoechst 33342 in the corresponding wells.

Assessment of caspase activation in live cells. The cells placed in an 8-chamber cell culture slide were impregnated with a CellEvent® caspase-3/7 green detection reagent (7.5 μM; #C10423, Thermo Fisher Scientific), a fluorogenic substrate for activated caspase-3/7, for 30 min at 37˚C, and fluorescence images were obtained using a Nikon Optiphot-2 microscope. This reagent is non-fluorescent because the DEVD peptide hinders the binding of the dye to DNA. However, after the activation of caspase-3/7 in apoptotic cells, the DEVD peptide is cleaved, enabling the dye to connect to DNA and produce a bright fluorogenic response.

Measurements of the total, healthy, and damaged mitochondrial masses. Cells in a 96-well flat-bottom culture plate were loaded with MitoTraker®Green FM (200 nM, #M7514, Thermo Fisher Scientific) for 30 min at 37˚C and placed in a normoxic or hypoxic CO_2 incubator in the presence or absence of AZM for 24 h. Thereafter, the hypoxic cells were reoxygenated in a normoxic CO_2 incubator for 3 h. The cells that were exposed to hypoxia or normoxia were stained with TMRM (250 nM) and Hoechst33342 (10 μg/ml; Sigma-Aldrich Japan) for 30 min at 37˚C, and the fluorescence intensities of MitoTraker®Green FM (Ex 485 nm, Em 535 nm), TMRM (Ex 531 nm, Em 600 nm), and Hoechst33342 (Ex 350 nm, Em 460 nm) were detected on a microplate fluorometer (PerkinElmer ArvoX2). The fluorescence intensities of MitoTracker®Green FM and TMRM were normalized to that of Hoechst 33342 in the corresponding wells. The normalized fluorescence intensity of MitoTracker®Green FM was defined as the cellular amount of the total (healthy plus damaged) mitochondria, which was the product of the number of mitochondria per cytoplasm and the average individual mitochondrial volume; data were expressed as percentages relative to cells exposed to normoxia without AZM and set as value A. The normalized fluorescence intensity of TMRM was outlined as the cellular amount of MMP-positive healthy mitochondria; the data were expressed as percentages relative to cells with normoxia and without AZM and set as value B. All the mitochondria in cells with normoxia and without AZM were assumed to be healthy and MMP-positive. Based on this assumption, the percentage of MMP-positive mitochondria was calculated by dividing B by A and multiplying by 100. The cellular amount of MMP-negative, damaged mitochondria was calculated by subtracting B from A.

Depletion of mitochondrial DNA. A549 cells devoid of mitochondrial DNA (A549 ρ^0) were prepared as described previously (24) by culturing the cells in DMEM supplemented with 10% FBS in the presence of ethidium bromide (50 ng/ml), sodium pyruvate (1 mM), and uridine (100 μg/ml) for >20 generations. The successful establishment of the A549 ρ^0 cell line was confirmed by polymerase chain reaction, using mitochondrial DNA-specific primers, as described in our previous study (25).

Statistical analysis. Data pertaining to the descriptive statistics for continuous variables are expressed as means ± the standard deviations. A P-value of <0.05 was considered statistically significant. All statistical analyses were performed using the Eazy R statistical software (version 1.54), which is available at https://www.jichi.ac.jp/saitama-sct/SaitamaHP.files/statmedEN.html (26). The statistical difference between two groups was calculated using the Welch t-test. Multiple comparisons between more than two groups were made using one-way ANOVA when a single variable was compared among groups or two-way ANOVA when two variables were compared simultaneously. If the results of the ANOVA were

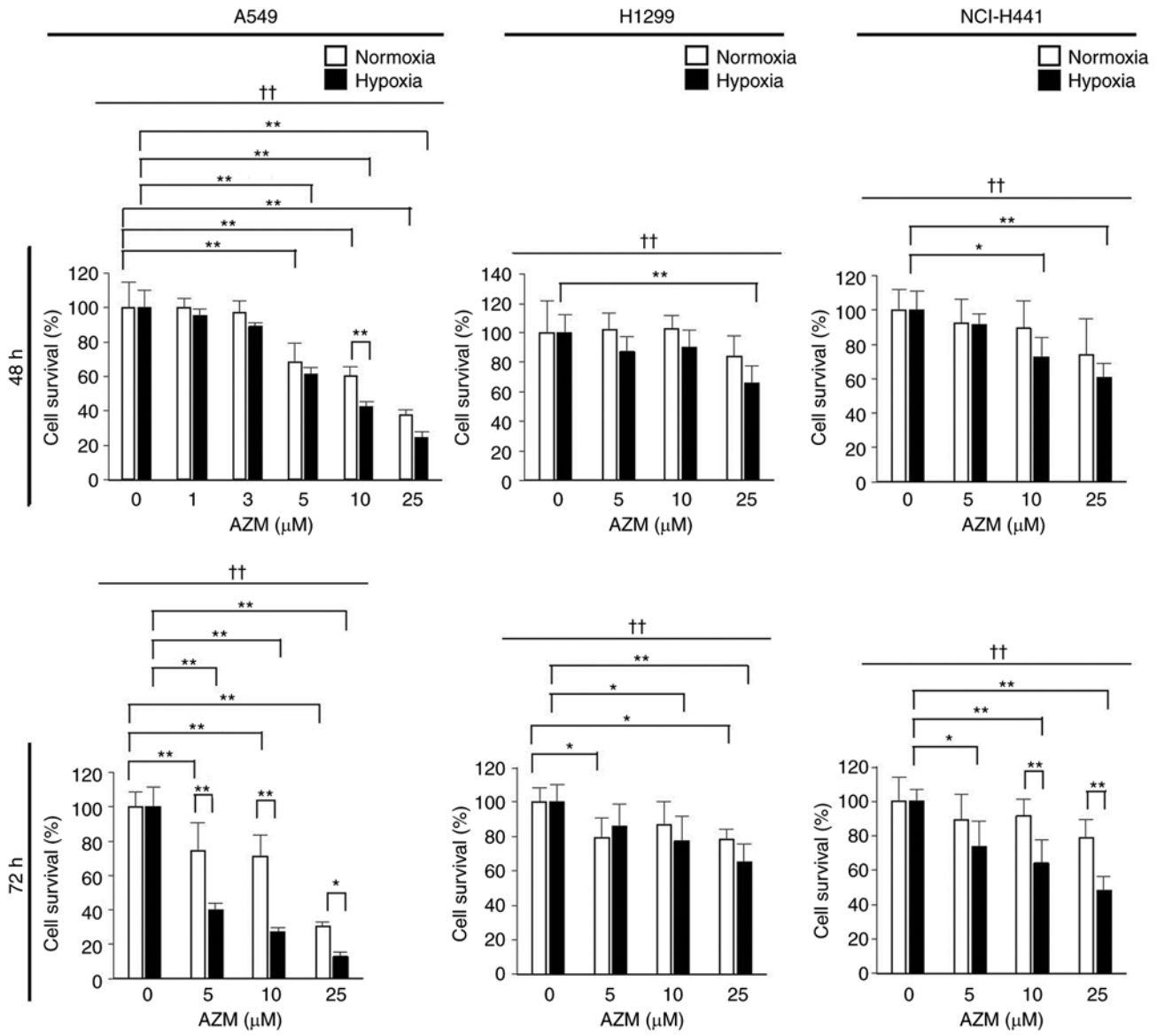

Figure 1. Dose-dependent and time-dependent effects of AZM on the survival rates of lung cancer cells under normoxic and hypoxic conditions. A549, H1299 and NCI-H441 cells were exposed to normoxia (20% O_2) or hypoxia (0.3% O_2) for 48 and 72 h in the presence or absence of AZM (1-25 μM) to study the effect of AZM on lung cancer cell survival under normoxic and hypoxic conditions. Cell survival was determined using the Hoechst 33342 DNA quantification assay. Data are presented as the mean and standard deviation (n=6). ††P<0.01 (two-way ANOVA). *P<0.05 and **P<0.01 (Tukey's test). Each panel shows the representative data of three independent experiments. AZM, azithromycin.

significant, Tukey's test was used as a post hoc test for multiple comparisons. The required sample size was determined based on our preliminary experiments and the relevant literature (13-16).

Results

AZM reduces the survival of lung cancer cells exposed to hypoxia. AZM treatment under normoxia (20% O_2) had minimal impact on the survival of H1299 and NCI-H441 cells but significantly reduced that of A549 cells, indicating that susceptibility to AZM cytotoxicity was cell-type specific (Fig. 1). However, AZM treatment tended to diminish the survival rates of all the tested cell types more effectively under hypoxic (0.3% O_2) conditions than under normoxic conditions, indicating that the cytotoxic action of AZM was enhanced under hypoxia. The A549 cells were used in subsequent experiments because they were found to be the most susceptible to AZM treatment.

AZM induces apoptosis under hypoxic conditions. The morphologies of A549 cells stained with Diff-quick and DAPI showed that AZM treatment along with exposure to hypoxia induced apoptosis (characterized by nuclear condensation and fragmentation with cytoplasmic shrinkage) (Fig. 2A-D). Immunofluorescence staining revealed that AZM treatment with hypoxia exposure induced caspase-3 cleavage (Fig. 2E). Furthermore, AZM treatment with hypoxia exposure stimulated the cleavage of PARP and caspase-3 in the Western blot analysis (Fig. 2F). These results indicated that AZM treatment induced apoptosis under hypoxic conditions. The reduction in the cell survival rate triggered by the aforementioned measures

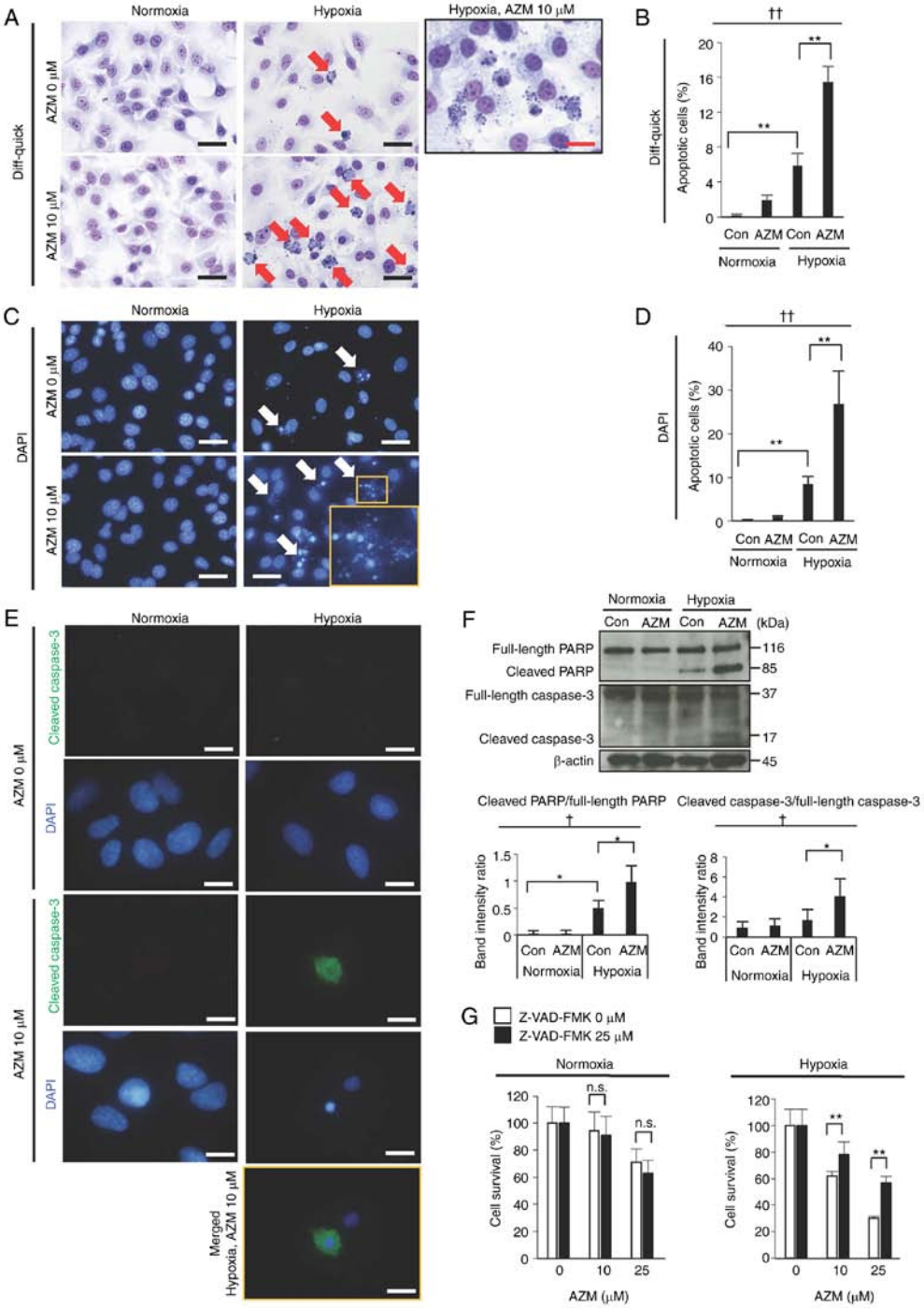

Figure 2. Effect of AZM on the apoptosis of A549 cells under normoxia or hypoxia. (A) Representative images of Diff-quick-stained A549 cells exposed to normoxia (20% O_2) or hypoxia (0.3% O_2) for 48 h in the presence or absence of AZM (10 μM). Red arrows indicate apoptotic cells exhibiting nuclear condensation and fragmentation with cytoplasmic shrinkage. The box shows a magnified image of apoptotic cells observed after hypoxia exposure in the presence of AZM. Black scale bar, 20 μm; red scale bar, 10 μm. (B) Quantitative analysis of apoptotic cells in Diff-quick-stained A549 cells exposed to normoxia (20% O_2) or hypoxia (0.3% O_2) for 48 h in the presence or absence of AZM (10 μM). Data are presented as the mean and standard deviation (n=4). ††P<0.01 (one-way ANOVA). **P<0.01 (Tukey's test). (C) Representative fluorescence microscopy images of A549 cells exposed to normoxia or hypoxia for 48 h in the presence or absence of AZM (10 μM). Cell nuclei were stained with DAPI (blue). Scale bar, 20 μm. White arrows indicate apoptotic cells exhibiting nuclear condensation and fragmentation. The right lower inset shows a magnified image of apoptotic cells. (D) Quantitative analysis of apoptotic cells in DAPI-stained A549 cells exposed to normoxia or hypoxia for 48 h in the presence or absence of AZM (10 μM). Data are presented as the mean and standard deviation (n=4). ††P<0.01 (one-way ANOVA). **P<0.01 (Tukey's test). (E) Cells were immunostained with anti-cleaved caspase-3 (green) and counterstained with DAPI (blue). Scale bar, 10 μm. A merged image is only included for the hypoxia + AZM group because the other groups showed no positive signal for cleaved caspase-3 in immunostaining. (F) Western blot analysis of the cleavage of PARP and caspase-3 in A549 cells exposed to normoxia or hypoxia for 48 h in the presence or absence of AZM (10 μM). The relative protein levels were semi-quantified using densitometry and expressed as the cleaved protein/full-length protein ratio. Data are presented as the mean and standard deviation (n=4). †P<0.05 (one-way ANOVA). *P<0.05 (Tukey's test). (G) To examine whether apoptosis is involved in reduced cell survival under hypoxic conditions with AZM treatment, A549 cells were exposed to normoxia or hypoxia for 48 h with or without AZM treatment (10 or 25 μM) in the presence or absence of Z-VAD-FMK (25 μM). The cell survival rate was calculated using the Hoechst 33342 DNA quantification assay. Data are presented as the mean and standard deviation (n=6). The representative results of three independent experiments are shown. **P<0.01 vs. cells not treated with Z-VAD-FMK (Welch t-test). AZM, azithromycin; Con, control; PARP, poly[ADP-ribose]polymerase 1; Z-VAD-FMK, benzyloxycarbonyl-L-valyl-L-alanyl-[(2S)-2-amino-3-(methoxycarbonyl)propionyl]fluoromethane; n.s., not significant.

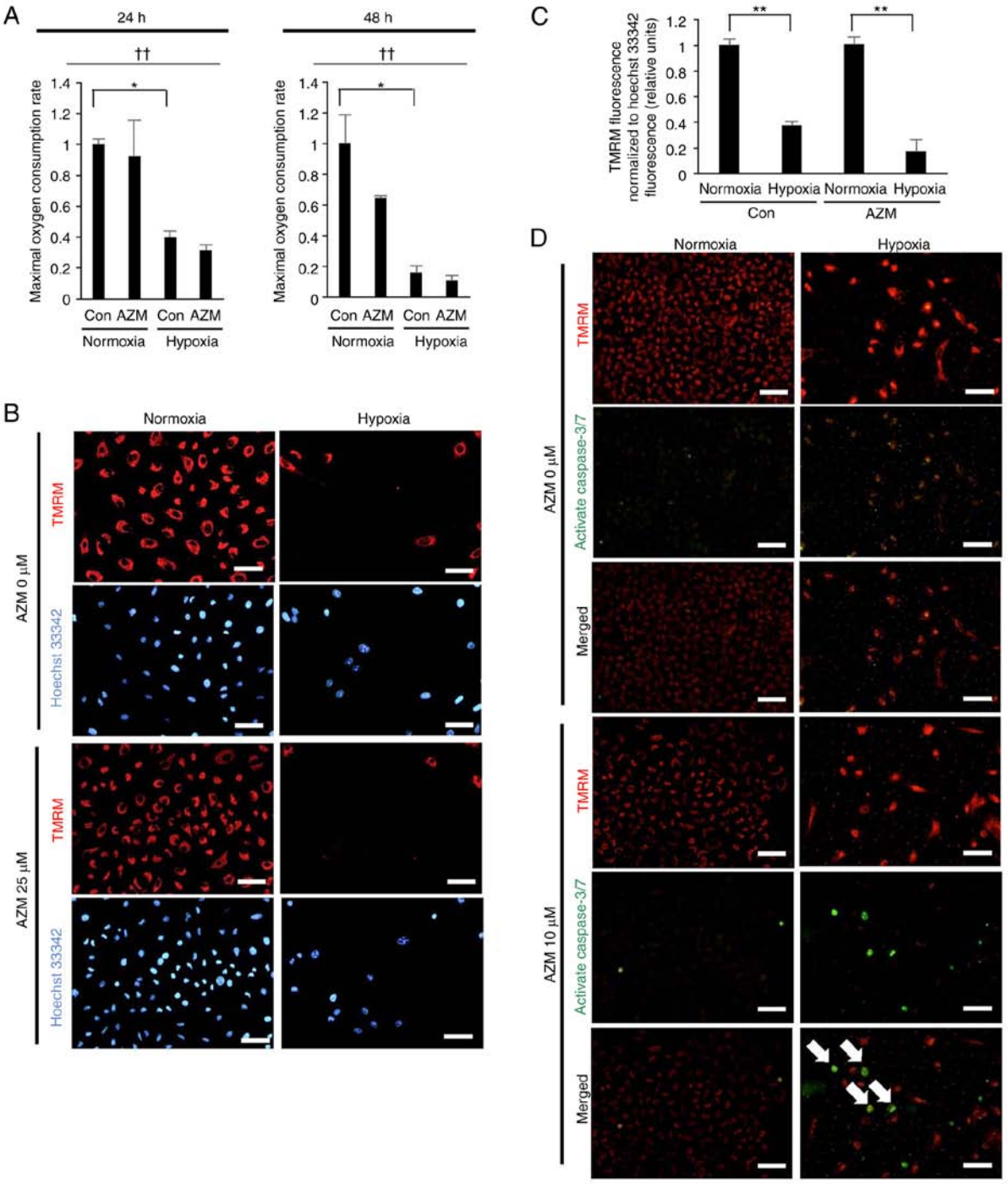

Figure 3. Effect of hypoxia on mitochondrial damage and apoptosis in A549 cells in the presence or absence of AZM. A549 cells were exposed to either normoxia (20% O_2) or hypoxia (0.3% O_2) for (A) 24 and 48 h, (B and C) 24 h, and (D) 48 h in the presence or absence of AZM (10 μM). After 3 h of reoxygenation, the mitochondrial function and apoptosis were assessed. (A) The maximal oxygen consumption rate was measured using a Seahorse XFp analyzer in the presence of the mitochondrial uncoupler carbonyl cyanide 4-(trifluoromethoxy)phenylhydrazone (0.5 μM). Data are presented as the mean and standard deviation (n=3). ††P<0.01 (two-way ANOVA). *P<0.05 (Tukey's test). The representative results of three independent experiments are shown. (B and C) The mitochondrial membrane potential was evaluated by staining with TMRM (red) and fluorescence images were acquired. Cell nuclei were stained with Hoechst 33342 (blue). (B) Representative data of four independent experiments are shown. Scale bar, 40 μm. (C) Quantitative analysis of TMRM fluorescence normalized to Hoechst 33342 fluorescence. Data are presented as the mean and standard deviation (n=6). **P<0.01 (Welch t-test). (D) The cells were co-stained with TMRM (red) and the CellEvent® caspase-3/7 green detection reagent (green), a fluorogenic substrate for activated caspase-3/7 to determine whether hypoxic mitochondrial damage in the presence or absence of AZM was associated with apoptosis. Scale bar, 40 μm. The representative results of three independent experiments are shown. Some cells stained negatively with TMRM under hypoxic conditions exhibited apoptosis in the presence of AZM (arrows). AZM, azithromycin; Con, control; TMRM, tetramethylrhodaminemethyl ester.

was attenuated in the presence of the pan-caspase inhibitor, Z-VAD-FMK (Fig. 2G). A549 cells treated with AZM demonstrated a moderate (but significant) decrease in cell survival even under normoxic conditions (Fig. 1). However, under the latter, no evidence of apoptosis induction by AZM treatment (Fig. 2A-D) or the improvement in cell survival in the presence

of Z-VAD-FMK (Fig. 2G), suggesting that hypoxia is a prerequisite for apoptosis induction by AZM.

Hypoxia exposure induces sustained mitochondrial damage. Mitochondrial damage is known to elicit apoptosis (27); therefore, the effect of hypoxia exposure on the induction of mitochondrial damage in lung cancer cells was assessed in this study. The A549 cells, which were exposed to hypoxia for 24 h or 48 h and had returned to normoxia for 3 h prior to the assay, exhibited marked reductions in their maximal oxygen consumption capacity (Fig. 3A) and MMP (Fig. 3B and C). These results indicated that hypoxia exposure promoted mitochondrial damage that was sustained even after reoxygenation. Additionally, the loss of MMP after exposure to hypoxia was associated with apoptosis induction in the presence, but not absence, of AZM (Fig. 3D), indicating that hypoxia-induced mitochondrial damage resulted in apoptosis induction only when AZM was present.

AZM inhibits the autophagy and mitophagy flux by inducing lysosomal dysfunction in lung cancer cells exposed to hypoxia. Damaged mitochondria are known to be effectively removed by mitophagy (28-31). Western blot analyses demonstrated that hypoxia exposure in the absence of AZM decreased the autophagy substrate, p62, and the mitochondrial proteins, HSP60 and UQCRC1, but increased the autophagosomal marker, LC3B-II (Fig. 4A). However, the presence of AZM inhibited the hypoxia-induced reductions in p62 and HSP60 and markedly increased the level of LC3B-II, suggesting that AZM treatment inhibited the autophagy and mitophagy flux promoted by hypoxia. Fluorescent small molecules that differentially stained autophagosomes and autolysosomes were used to confirm the findings of the Western blot analysis. DAL®Green and DAP®Red cross the plasma membranes of living cells and are incorporated in the autophagosome. DAL®Green fluorescence becomes stronger after a lysosome fuses with an autophagosome due to the increase in the acidity, whereas DAP®Red fluorescence remains unchanged. The hypoxic A549 cells displayed much stronger DAP®Red fluorescence than the normoxic cells (which reflected the elevated formation of autophagosomes and/or autolysosomes) and much stronger DAL®Green fluorescence with a bright fluorescent punctate (which was indicative of the formation of acidic autolysosomes) (Fig. 4B). However, in the presence of AZM, the hypoxic cells showed weak DAL®Green fluorescence without any bright fluorescent punctate while the DAP®Red fluorescence remained unchanged. These results indicated that hypoxia stimulated the formation of autophagosome/autolysosomes, whereas AZM treatment blocked this process. Mtphagy®Dye and Lyso®Dye, which accumulate in intact mitochondria and lysosomes, respectively, were used in this study. The mitophagosome fuses to the lysosome to form a mitolysosome when mitophagy is induced, and the Mtphagy®Dye emits a strong red fluorescence due to the resultant acidity. Hypoxic cells demonstrated brighter Mtphagy®Dye punctate compared to normoxic cells, indicating a higher number of mitolysosomes (Fig. 4C). However, in the presence of AZM, the hypoxia-induced punctuation of Mtphagy®Dye almost disappeared, proving that AZM treatment had inhibited the formation of acidic mitolysosomes. Furthermore, the Lyso®Dye fluorescence was more common in the presence of AZM than in its absence, irrespective of normoxia and hypoxia (Fig. 4C). These findings implied that AZM treatment had blocked acidic mitolysosome formation via lysosomal dysfunction but not via lysosome disappearance. Therefore, we next assessed the lysosomal pH using the pHLys®Red dye, which accumulates in lysosomes, and emits intense fluorescence, as the acidity increases. As shown in Fig. 4D, pHLys®Red fluorescence almost diminished in the presence of AZM, irrespective of normoxia, or hypoxia exposure, showing that normal lysosome acidification was impaired by AZM treatment. Overall, these findings revealed that AZM treatment inhibited hypoxia-induced mitophagy via lysosomal dysfunction, probably due to the increase in the lysosomal pH.

AZM treatment induces the accumulation of damaged mitochondria under hypoxic conditions. Based on these findings, we assumed that AZM treatment under hypoxic conditions induced the cellular accumulation of damaged mitochondria via the inhibition of the mitophagy flux, which eventually induced apoptosis. To test this assumption, we estimated the abundance of total mitochondria (healthy plus damaged mitochondria) stained positive for Mito®Tracker Green, MMP-positive healthy mitochondria stained positive for TMRM, and MMP-negative, damaged mitochondria stained negative for TMRM. Hypoxia exposure in the absence of AZM decreased the percentage of MMP-positive healthy mitochondria among all mitochondria (Fig. 5A). Hypoxia exposure in the presence of AZM decreased the proportion of MMP-positive healthy mitochondria and markedly increased the cellular amount of damaged mitochondria and also that of all mitochondria. These results indicated that hypoxia exposure induced the cellular accumulation of damaged mitochondria, particularly in the presence of AZM. The mitophagy cargo receptors BNIP3 and BNIP3L/Nix, which are highly expressed on the mitochondrial outer membrane during hypoxia, transmit a mitophagy signal to degrade mitochondria that are either damaged or superfluous due to reduced oxygen supply (32-37). Western blot analyses demonstrated that hypoxia exposure elevated the cellular amounts of BNIP3 and BNIP3L/Nix, which was more evident in the presence of AZM than in its absence (Fig. 5B), and suggested the inhibition of the degradation of mitochondria expressing BNIP3 and BNIP3L/Nix. Collectively, these results indicated that the cellular accumulation of damaged mitochondria observed in hypoxic lung cancer cells was attributable, at least in part, to the inefficient removal of damaged (or superfluous) mitochondria due to the AZM-induced inhibition of mitophagy. To verify if the accumulation of damaged mitochondria (which should have been targeted for degradation) had caused the increase in the cell death rare after AZM treatment under hypoxic conditions, we evaluated the effect of AZM on the survival of mitochondria-deficient A549 cells (ρ^0 cells). In contrast to the control A549 cells, ρ^0 A549 cells exhibited complete resistance to AZM cytotoxicity during hypoxia, indicating that mitochondrial homeostasis disturbances play an important role in the anticancer effect of AZM under hypoxic conditions (Fig. 5C).

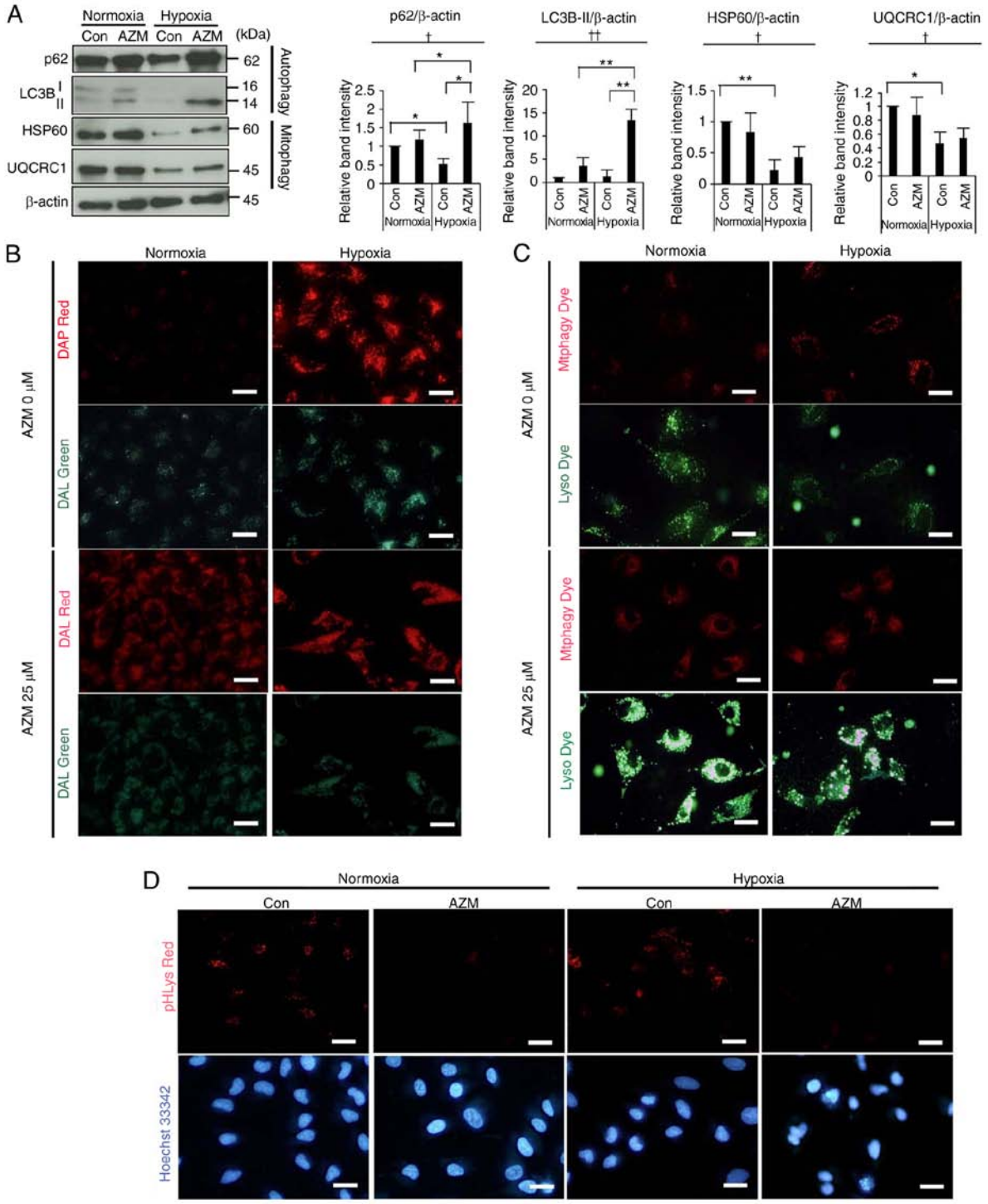

Figure 4. Effect of AZM on the autophagy and mitophagy flux under normoxic or hypoxic conditions. A549 cells were subjected to either normoxia (20% O_2) or hypoxia (0.3% O_2) for (B-D) 24 or (A) 48 h in the presence or absence of AZM (A, 10 μM; B-D, 25 μM). (A) Western blot analysis of the autophagy substrate p62, the autophagosomal marker LC3B, and the mitochondrial abundance markers HSP 60 and UQCRC1. Band intensities were normalized to β-actin expression and data were summarized in the graphs on the right. Data are presented as the mean and standard deviation (n=3). †P<0.05 and ††P<0.01 (one-way ANOVA). *P<0.05 and **P<0.01 (Tukey's test). (B) Representative images for the detection of the autophagy flux by staining with DAP®Red (red) and DAL®Green (green). Scale bar, 20 μm. (C) Representative images for the detection of the mitophagy flux by staining with Mtphagy®Dye (red) and Lyso®Dye (green). Scale bar, 20 μm. (D) Representative images for the detection of lysosomal acidification by staining with pHLys®Red. Scale bar, 20 μm. AZM, azithromycin; Con, control; HSP 60, heat shock protein 60; UQCRC1, ubiquinol-cytochrome b-c1 complex subunit 1.

Discussion

In the present study, AZM treatment of lung cancer cells under hypoxic conditions induced the accumulation of damaged mitochondria via mitophagy inhibition, eventually leading to apoptosis. Hypoxia plays a vital role in cancer progression and therapeutic resistance (38,39). It is reported to damage mitochondria and activate mitophagy to remove the organelles (40-42). In line with this, hypoxia exposure promoted mitochondrial damage in lung cancer cells, which utilized

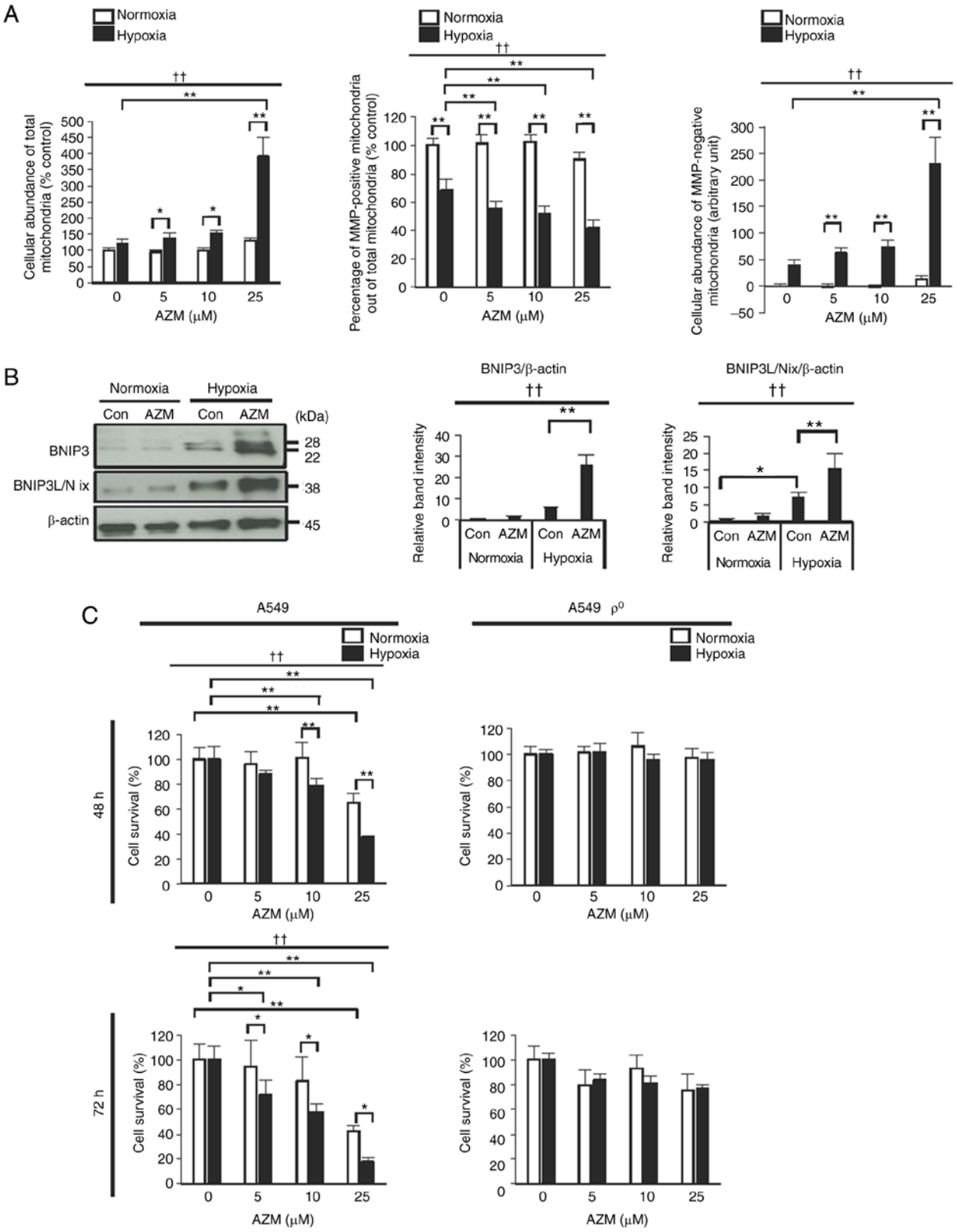

Figure 5. Effect of AZM on mitochondrial homeostasis under normoxic and hypoxic conditions. (A) A549 cells were loaded with MitoTraker®Green and exposed to normoxia or hypoxia in the presence or absence of AZM (5, 10, and 25 μM) for 48 h to study the effect of AZM on the cellular abundance of total, MMP-positive and MMP-negative mitochondria. The MMP-positive mitochondria were stained with TMRM and the fluorescence intensities of MitoTraker®Green FM (a marker of the total mitochondrial mass) and TMRM (a marker of healthy mitochondria) were measured and normalized to the fluorescence intensity of Hoechst 33342. Data are presented as the mean and standard deviation (n=6). ††P<0.01 (two-way ANOVA). *P<0.05 and **P<0.01 (Tukey's test). (B) Western blot analysis of BNIP3 and BNIP3L/Nix in A549 cells exposed to normoxia or hypoxia for 48 h with or without AZM (10 μM). Data are presented as the mean and standard deviation (n=3). ††P<0.01 (one-way ANOVA). *P<0.05 and **P<0.01 (Tukey's test). (C) Control A549 cells and A549 cells devoid of mitochondrial DNA (A549 ρ^0 cells) treated with normoxia or hypoxia for 48 and 72 h in the presence or absence of AZM (5-25 mM). Data are presented as the mean and standard deviation (n=6). ††P<0.01 (two-way ANOVA). *P<0.05 and **P<0.01 (Tukey's test). Each panel shows the representative data of three independent experiments. AZM, azithromycin; Con, control; MMP, mitochondrial membrane potential; TMRM, tetramethylrhodaminemethyl ester; BNIP3, Bcl-2/E1B-19kDa-interacting protein 3; BNIP3L/Nix, Bcl-2/E1B-19kDa-interacting protein 3-like.

mitophagy to remove the damaged (or superfluous) organelles to maintain mitochondrial homeostasis in the current study. More importantly, AZM exerted anticancer effects under hypoxic conditions, which was attributed to the AZM-induced mitolysosome dysfunction and the increase in the lysosomal pH that led to impaired removal of the damaged mitochondria and eventually induced apoptosis. Our findings highlight AZM as a promising anticancer drug that exploits tumor hypoxia and interferes with the mitochondrial homeostasis required to maintain cell survival under hypoxic conditions.

The role of mitophagy in tumor biology is complex and depends on the tumor type and TME (8,9,37). Mitophagy generally promotes cancer cell survival by removing damaged mitochondria and reducing reactive oxygen species production. Conversely, it may reduce the cancer cell survival rate by inducing mitophagy-dependent cell death. The findings of the current study display that the activation of mitophagy in cancer cells exposed to hypoxia provides a self-defense mechanism that helps their survival. Based on these findings, we propose the inhibition of mitophagy as a therapeutic target for cancer cells surviving in hypoxic TMEs.

Hypoxia is the key factor in mitochondrial damage and dysfunction (28,42). Profound reductions in the mitochondrial oxygen consumption rate and MMP were observed in the present study, which persisted after reoxygenation following hypoxia. Unfortunately, it was not possible to determine whether the mitochondrial dysfunction was due to hypoxia and/or hypoxia-reoxygenation damage because the mitochondrial function was assessed under atmospheric air following hypoxia exposure. Nonetheless, some regions in solid tumors have been reported to exhibit chronic hypoxia due to impaired oxygen diffusion, while others are subjected to transient hypoxia, i.e., hypoxia-reoxygenation, due to the cyclic opening and closing of tumor vessels (39). Furthermore, hypoxia was found to stimulate the autophagy and mitophagy flux in the present study, corroborating the findings of a previous study (41). The hypoxia-stimulated mitophagy flux appears to be beneficial for hypoxic cancer cells by eliminating damaged and dysfunctional mitochondria that are potentially harmful to the cell and adapting the overall mitochondrial mass to the decreased oxygen supply.

In line with previous studies (including our own) (14-17,43), AZM suppressed the autophagy flux in the current study; in addition, a decrease in the mitophagy flux was observed for the first time in the present study. AZM treatment induced mitolysosome dysfunction and an increase in the lysosomal pH. Under hypoxic conditions, this led to the accumulation of damaged (or superfluous) mitochondria, which may have induced apoptosis. Additionally, the increase in the hypoxia-related mitophagy cargo receptors BNIP3 and BNIP3L/Nix (9,32-37,41) in the presence of AZM was more marked than that in its absence. These data are interpreted as follows: hypoxia stimulates the mitochondrial expression of BNIP3 and BNIP3L/Nix, which transmits a mitophagy signal to remove damaged (or superfluous) mitochondria; however, in the presence of AZM, the BNIP3- and BNIP3L/Nix-expressing mitochondria are accumulated in abnormal pattern due to blocking of the downstream mitolysosome formation. The precise molecular mechanism by which AZM inhibits the autophagy and mitophagy flux remains unclear. In line with the findings of a previous study (43), AZM impaired the acidification of auto- and mitolysosomes with raised lysosomal pH, suggesting that vacuolar (V)-type ATPase may be a candidate target molecule of AZM therapy. The other potential targets of AZM therapy reportedly include valosin-containing protein/p97 (44), keratin-18, and α/β-tubulin (19).

Mitochondrial damage is the most well-known inducer of apoptosis. Therefore, we speculated that AZM treatment stimulated apoptosis under hypoxic conditions following the accumulation of damaged mitochondria that were not eliminated due to the AZM-induced inhibition of mitophagy. In addition to mitochondrial damage, lysosomal dysfunction is reported to cause apoptosis that may or may not be dependent on the mitochondria. Recent studies (including ours) have demonstrated that AZM treatment induces apoptosis in lung cancer cells exposed to DNA-damaging drugs via lysosomal membrane permeabilization (LMP) by lysophagy inhibition (16,45). Lysosome damage may also affect other types of autophagy, such as endoplasmic reticulum-phagy and peroxphagy. LMP is capable of inducing apoptosis via the mitochondria-independent pathway (46). However, mitochondria-independent mechanisms, such as LMP-mediated non-mitochondrial apoptosis, were unlikely to play a role in the present study because mitochondrion-deficient A549 cells (ρ^0 cells) exhibited complete resistance to the cytotoxic action of AZM during hypoxia exposure, validating our notion that the accumulation of damaged mitochondria plays a primary role in the induction of apoptosis by AZM treatment under hypoxic conditions.

In the present study, the cytotoxic efficacy of AZM was estimated differently by Hoechst 33342 DNA quantification and apoptosis assays. For example, in A549 hypoxic cells treated with 10-μM AZM for 48 h, around 55% of the cells did not survive in the Hoechst 33342 DNA quantification assay, whereas only 15-25% of then were found to be apoptotic. Furthermore, in A549 cells treated with 10-μM AZM for 48 h under normoxic conditions, around 30% of the cells were dead in the Hoechst 33342 DNA quantification assay, whereas less than 5% of the cells turned out to be apoptotic. We think there are two possible reasons why the rate of apoptotic cell death is lower than the percentages of cell death estimated in the Hoechst 33342 DNA quantification assay. First, apoptotic cells that had detached from the surfaces of the cell culture plates were washed away during cell fixation for the Diff-quick and DAPI staining methods. Second, non-apoptotic cell death, such as necrosis and necroptosis, was involved in cell death induced by AZM under normoxic and hypoxic conditions.

Furthermore, there were some variations in cell survival between different experiments. Although not conclusive, these variations may be attributed to different cell confluencies. In additional experiments, we found that cell survival increased as the initial plating cell density increased. Thus, we suspect that cell-to-cell contact or cell-derived soluble substances may affect cell survival and contribute, in part, to the observed variations in cell survival. However, AZM consistently reduced cell survival under hypoxic conditions at all the cell densities tested, which supports our conclusion (data not shown).

Some bleedthrough was observed in the fluorescence images when cells were co-stained with TMRM and the CellEvent® caspase-3/7 green detection reagent, following

treatment with AZM for 48 h. This was the result of the optical system on our microscope; however, this did not affect the interpretation of the results. We could not quantify the results of the detection of the autophagy flux by staining with DAP®Red and DAL®Green and the detection of the mitophagy flux by staining with Mtphagy®Dye and Lyso®Dye because of the following technical reasons. First, the fluorescence intensities from fluorochromes were too weak to be measured using a conventional microplate fluorometer. Second, it was difficult to count the number of small fluorescent punctuates, which indicated increased formation of acidic autolysosomes, using a fluorescent microscope, because they were some and often formed aggregates.

In contrast to the control A549 cells, ρ^0 A549 cells exhibited complete resistance to AZM cytotoxicity during hypoxia. We interpreted the results of the experiments with ρ^0 A549 cells as follows: no mitochondrial DNA => no mitochondrial translation => no functional mitochondria => no mitochondrial respiration or electron transfer => hypoxia resistance => resistance to AZM under hypoxia. We believe that AZM resistance during hypoxia in ρ^0 A549 cells indicates that disturbances in functional mitochondria in control A549 cells play an important role in the anticancer effect of AZM under hypoxic conditions.

In addition to its high cytotoxic effect under hypoxic conditions, AZM exerted weak but significant cytotoxicity under normoxic conditions without any strong induction of apoptosis. Furthermore, the cytotoxic effect of AZM under hypoxic conditions was not completely abolished in the presence of the pan-caspase inhibitor, Z-VAD-FMK. These findings suggest that AZM may promote apoptotic and non-apoptotic cell death. For example, previous studies showed that AZM potentiated the anticancer effects of epidermal growth factor receptor tyrosine kinase inhibitors and lansoprazole by inducing necroptosis (14) and necrosis (47), respectively.

In the present study, H1299 and HCI-H441 cells were less susceptible to the cytotoxic effect of AZM under hypoxic conditions than A549 cells. The reasons for the different susceptibilities between the cell lines remain unclear. However, the lower susceptibilities of H1299 and NCI-H441 cells to AZM cytotoxicity under hypoxic conditions may be the result of genetic deletion because they carry a mutant *p53* gene, whereas A549 cells carry a wild-type *p53* gene (48).

Hypoxia in the TME is proposed to be a new target for cancer therapy. Hypoxia-targeted drugs in pre-clinical and clinical trials include nanoparticle oxygen carriers and generators, hypoxia-activated prodrugs, and hypoxia-inducible factor (HIF) inhibitors (5,6). However, many of these compounds cannot be used due to side effects or failure in the aforementioned studies. Furthermore, HIF inhibition, arguably the most attractive tactics, could have serious side effects because HIFs are highly expressed in cancer cells and some normal tissues. AZM has been widely and safely used in clinical practice to treat infectious and non-infectious diseases, such as bacterial infection, and bronchiectasis. A recent *in vivo* study using a murine xenograft model with A549 cells revealed that daily oral AZM administration suppressed autophagy and the growth of tumor cells; however, the relation between this effect and tumor hypoxia was not determined (19).

In conclusion, this study shows, for the first time, that AZM can target mitochondrial damage in hypoxic tumor cells by inhibiting mitophagy. Additional studies are required to validate these findings and determine their effect in the clinical setting.

Acknowledgements

The authors would like to thank Mrs. Eriko Kurosawa (Tokyo Medical University Ibaraki Medical Center, Ami-machi, Ibaraki, Japan) for providing technical assistance.

Funding

This work was supported by a Grant-in-Aid for Scientific Research from the Ministry of Education and Science, Japan (grant no. 21K08189); Nippon Boelinger Ingelheim Co., Ltd., Chugai Pharmaceutical Co., Ltd.; Daiichi Sankyo, Inc.; Kyowa Kirin Co., Ltd.; Eli Lilly Japan K. K.; Shionogi & Co., Ltd.; and Takeda Pharmaceutical Co., Ltd.

Availability of data and materials

The datasets used and/or analyzed during the current study are available from the corresponding author on reasonable request.

Authors' contributions

KT and KA conceived and designed the project, acquired, analyzed and interpreted the data, and wrote the original draft. TO, SA and HN analyzed and interpreted the data. KT and KA confirmed the authenticity of all the raw data. All authors read and approved the final manuscript.

Ethics approval and consent to participate

Not applicable.

Patient consent for publication

Not applicable.

Competing interests

The authors declare that they have no competing interests.

References

1. Vaupel P, Mayer A and Höckel M: Tumor hypoxia and malignant progression. Methods Enzymol 381: 335-354, 2004.
2. Finicle BT, Jayashankar V and Edinger AL: Nutrient scavenging in cancer. Nat Rev Cancer 18: 619-633, 2018.
3. Jain RK: Antiangiogenesis strategies revisited: From starving tumors to alleviating hypoxia. Cancer Cell 26: 605-622, 2014.
4. Whatcott CJ, Han H and Von Hoff DD: Orchestrating the tumor microenvironment to improve survival for patients with pancreatic cancer: Normalization, not destruction. Cancer J 21: 299-306, 2015.
5. Chen Z, Han F, Du Y, Shi H and Zhou W: Hypoxic microenvironment in cancer: Molecular mechanisms and therapeutic interventions. Signal Transduct Target Ther 8: 70, 2023.
6. Zhuang Y, Liu K, He Q, Gu X, Jiang C and Wu J: Hypoxia signaling in cancer: Implications for therapeutic interventions. MedComm (2020) 4: e203, 2023.

7. Mizushima N and Komatsu M: Autophagy: Renovation of cells and tissues. Cell 147: 728-741, 2011.
8. Levy JMM, Towers CG and Thorburn A: Targeting autophagy in cancer. Nat Rev Cancer 17: 528-542, 2017.
9. Xie Y, Liu J, Kang R and Tang D: Mitophagy receptors in tumor biology. Front Cell Dev Biol 8: 594203, 2020.
10. Green DR and Llambi F: Cell death signaling. Cold Spring Harb Perspect Biol 7: a006080, 2015.
11. Denton D and Kumar S: Autophagy-dependent cell death. Cell Death Differ 26: 605-616, 2019.
12. Hassan SN, Mohamed Yusoff AA, Idris Z, Mohd Redzwan N and Ahmad F: A mini-review on anticancer-related properties of azithromycin and its potential activities in overcoming the challenges of glioblastoma. Fundam Clin Pharmacol 37: 918-927, 2023.
13. Moriya S, Komatsu S, Yamasaki K, Kawai Y, Kokuba H, Hirota A, Che X, Inazu M, Gotoh A, Hiramoto M and Miyazawa K: Targeting the integrated networks of aggresome formation, proteasome, and autophagy potentiates ER stress-mediated cell death in multiple myeloma cells. Int J Oncol 46: 474-486, 2015.
14. Mukai S, Moriya S, Hiramoto M, Kazama H, Kokuba H, Che X, Yokoyama T, Sakamoto S, Sugawara A, Sunazuka T, *et al*: Macrolides sensitize EGFR-TKI-induced non-apoptotic cell death via blocking autophagy flux in pancreatic cancer cell lines. Int J Oncol 48: 45-54, 2016.
15. Tanaka H, Hino H, Moriya S, Kazama H, Miyazaki M, Takano N, Hiramoto M, Tsukahara K and Miyazawa K: Comparison of autophagy inducibility in various tyrosine kinase inhibitors and their enhanced cytotoxicity via inhibition of autophagy in cancer cells in combined treatment with azithromycin. Biochem Biophys Rep 22: 100750, 2020.
16. Toriyama K, Takano N, Kokuba H, Kazama H, Moriya S, Hiramoto M, Abe S and Miyazawa K: Azithromycin enhances the cytotoxicity of DNA-damaging drugs via lysosomal membrane permeabilization in lung cancer cells. Cancer Sci 112: 3324-3337, 2021.
17. Qiao X, Wang X, Shang Y, Li Y and Chen SZ: Azithromycin enhances anticancer activity of TRAIL by inhibiting autophagy and up-regulating the protein levels of DR4/5 in colon cancer cells in vitro and in vivo. Cancer Commun (Lond) 38: 43, 2018.
18. Asakura E, Nakayama H, Sugie M, Zhao YL, Nadai M, Kitaichi K, Shimizu A, Miyoshi M, Takagi K, Takagi K and Hasegawa T: Azithromycin reverses anticancer drug resistance and modifies hepatobiliary excretion of doxorubicin in rats. Eur J Pharmacol 484:333-339, 2004.
19. Takano N, Hiramoto M, Yamada Y, Kokuba H, Tokuhisa M, Hino H and Miyazawa K: Azithromycin, a potent autophagy inhibitor for cancer therapy, perturbs cytoskeletal protein dynamics. Br J Cancer 128:1838-1849, 2023.
20. Fiorillo M, Tóth F, Sotgia F and Lisanti MP: Doxycycline, azithromycin and vitamin C (DAV): A potent combination therapy for targeting mitochondria and eradicating cancer stem cells (CSCs). Aging (Albany NY) 11: 2202-2216, 2019.
21. Ozkan T, Hekmatshoar Y, Karabay AZ, Koc A, Altinok Gunes B, Karadag Gurel A, and Sunguroglu A: Assessment of azithromycin as an anticancer agent for treatment of imatinib sensitive and resistant CML cells. Leuk Res 102:106523, 2021.
22. Hassan SN, Mohamed Yusoff AA, Idris Z, Mohd Redzwan N and Ahmad F: Exploring the cytotoxicity and anticancer effects of doxycycline and azithromycin on human glioblastoma multiforme cells. Neurol Res 44: 242-251, 2022.
23. Hill BG, Benavides GA, Lancaster JR Jr, Ballinger S, Dell'talia L, Jianhua Z and Darley-Usmar VM: Integration of cellular bioenergetics with mitochondrial quality control and autophagy. Biol Chem 393: 1485-1512, 2012.
24. Brar SS, Meyer JN, Bortner CD, Van Houten B and Martin WJ II: Mitochondrial DNA-depleted A549 cells are resistant to bleomycin. Am J Physiol Lung Cell Mol Physiol 303: L413-L424, 2012.
25. Kikuchi R, Iwai Y, Tsuji T, Watanabe Y, Koyama N, Yamaguchi K, Nakamura H and Aoshiba K: Hypercapnic tumor microenvironment confers chemoresistance to lung cancer cells by reprogramming mitochondrial metabolism in vitro. Free Radic Biol Med 134: 200-214, 2019.
26. Kanda Y: Investigation of the freely available easy-to-use software 'EZR' for medical statistics. Bone Marrow Transplant 48: 452-458, 2013.
27. Ricci C, Pastukh V, Leonard J, Turrens J, Wilson G, Schaffer D and Schaffer SW: Mitochondrial DNA damage triggers mitochondrial-superoxide generation and apoptosis. Am J Physiol Cell Physiol 294: C413-C422, 2008.
28. Sulkshane P, Ram J, Thakur A, Reis N, Kleifeld O and Glickman MH: Ubiquitination and receptor-mediated mitophagy converge to eliminate oxidation-damaged mitochondria during hypoxia. Redox Biol 45: 102047, 2021.
29. Liu L, Feng D, Chen G, Chen M, Zheng Q, Song P, Ma Q, Zhu C, Wang R, Qi W, *et al*: Mitochondrial outer-membrane protein FUNDC1 mediates hypoxia-induced mitophagy in mammalian cells. Nat Cell Biol 14: 177-185, 2012.
30. Band M, Joel A, Hernandez A and Avivi A: Hypoxia-induced BNIP3 expression and mitophagy: In vivo comparison of the rat and the hypoxia-tolerant mole rat, Spalax ehrenbergi. FASEB J 23: 2327-2335, 2009.
31. Zhang H, Bosch-Marce M, Shimoda LA, Tan YS, Baek JH, Wesley JB, Gonzalez FJ and Semenza GL: Mitochondrial autophagy is an HIF-1-dependent adaptive metabolic response to hypoxia. J Biol Chem 283: 10892-10903, 2008.
32. Fu ZJ, Wang ZY, Xu L, Chen XH, Li XX, Liao WT, Ma HK, Jiang MD, Xu TT, Xu J, *et al*: HIF-1α-BNIP3-mediated mitophagy in tubular cells protects against renal ischemia/reperfusion injury. Redox Biol 36: 101671, 2020.
33. Li Y, Zheng W, Lu Y, Zheng Y, Pan L, Wu X, Yuan Y, Shen Z, Ma S, Zhang X, *et al*: BNIP3L/NIX-mediated mitophagy: Molecular mechanisms and implications for human disease. Cell Death Dis 13: 14, 2021.
34. Shao Y, Liu Z, Liu J, Wang H, Huang L, Lin T, Liu J, Wei Q, Zeng H, He G and Li X: Expression and epigenetic regulatory mechanism of BNIP3 in clear cell renal cell carcinoma. Int J Oncol 54: 348-360, 2019.
35. Zhang J and Ney PA: Role of BNIP3 and NIX in cell death, autophagy, and mitophagy. Cell Death Differ 16: 939-946, 2009.
36. Sowter HM, Ratcliffe PJ, Watson P, Greenberg AH and Harris AL: HIF-1-dependent regulation of hypoxic induction of the cell death factors BNIP3 and NIX in human tumors. Cancer Res 61: 6669-6673, 2001.
37. Poole LP and Macleod KF: Mitophagy in tumorigenesis and metastasis. Cell Mol Life Sci 78: 3817-3851, 2021.
38. Jing X, Yang F, Shao C, Wei K, Xie M, Shen H and Shu Y: Role of hypoxia in cancer therapy by regulating the tumor microenvironment. Mol Cancer 18: 157, 2019.
39. Li Y, Zhao L and Li XF: Hypoxia and the tumor microenvironment. Technol Cancer Res Treat 20: 15330338211036304, 2021.
40. Sun Y, Wen F, Yan C, Su L, Luo J, Chi W and Zhang S: Mitophagy protects the retina against anti-vascular endothelial growth factor therapy-driven hypoxia via hypoxia-inducible factor-1α signaling. Front Cell Dev Biol 9: 727822, 2021.
41. Daskalaki I, Gkikas I and Tavernarakis N: Hypoxia and selective autophagy in cancer development and therapy. Front Cell Dev Biol 6: 104, 2018.
42. Wang S, Tan J, Miao Y and Zhang Q: Mitochondrial dynamics, mitophagy, and mitochondria-endoplasmic reticulum contact sites crosstalk under hypoxia. Front Cell Dev Biol 10: 848214, 2022.
43. Renna M, Schaffner C, Brown K, Shang S, Tamayo MH, Hegyi K, Grimsey NJ, Cusens D, Coulter S, Cooper J, *et al*: Azithromycin blocks autophagy and may predispose cystic fibrosis patients to mycobacterial infection. J Clin Invest 121: 3554-3563, 2011.
44. Nujić K, Smith M, Lee M, Belamarić D, Tomašković L, Alihodžić S, Malnar I, Polančec D, Schneider K and Eraković Haber V: Valosin containing protein (VCP) interacts with macrolide antibiotics without mediating their anti-inflammatory activities. Eur J Pharmacol 677: 163-172, 2012.
45. Yamashita G, Takano N, Kazama H, Tsukahara K and Miyazawa K: p53 regulates lysosomal membrane permeabilization as well as cytoprotective autophagy in response to DNA-damaging drugs. Cell Death Discov 8: 502, 2022.
46. Johansson AC, Appelqvist H, Nilsson C, Kågedal K, Roberg K and Öllinger K: Regulation of apoptosis-associated lysosomal membrane permeabilization. Apoptosis 15: 527-540, 2010.
47. Takeda A, Takano N, Kokuba H, Hino H, Moriya S, Abe A, Hiramoto M, Tsukahara K and Miyazawa K: Macrolide antibiotics enhance the antitumor effect of lansoprazole resulting in lysosomal membrane permeabilization-associated cell death. Int J Oncol 57: 1280-1292, 2020.
48. Lai SL, Perng RP and Hwang J: p53 gene status modulates the chemosensitivity of non-small cell lung cancer cells. J Biomed Sci 7: 64-70, 2000.